

Energy and Mass Utilization During Drag-Modulated Plasma Aerocapture

Charles L. Kelly
 University of Washington
 Seattle, WA 98105
 clk1391@uw.edu

Justin M. Little
 University of Washington
 Seattle, WA 98105
 littlej7@uw.edu

Abstract—An analytical model is presented to assess the utilization of atmospheric energy and mass by a magnetoshell plasma during aerocapture. An appropriate control volume describing the plasma is defined using single ion trajectory analysis in the dipole magnetic field. Equations of continuity and state are developed to describe the plasma interaction with the atmospheric flow. The populations and temperatures of ions, electrons, and magnetoshell neutrals are tracked and steady state results are obtained. A strong correlation is demonstrated between applied magnetic field strength and absorbed mass, confirming initial notions that the magnetoshell drag can be modulated by the magnet. The plasma is found to self-sustain with no input power from the spacecraft, though propellant injection is required on the order of 1 mg/s during the maneuver. The mass absorbed from the flow is observed to decrease with increasing velocity due to shrinking of the control volume and reduced charge exchange interaction. The percentage of incident atmospheric mass and energy absorbed by the plasma is determined to be between 1% and 33% across a spacecraft velocity range of 2–20 km/s and atmospheric density range of 10^{16} – 10^{18} m⁻³. That this percentage is not 100% indicates that some flow passes through the plasma without interaction, contrary to previous studies which assumed the plasma to be fully opaque.

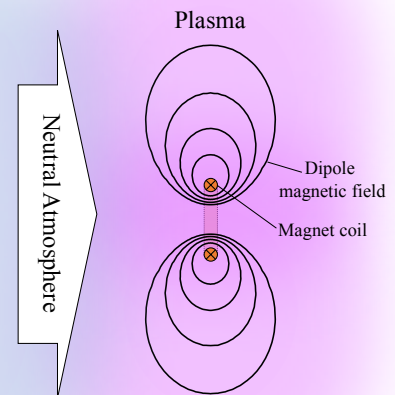


Figure 1. Cross section view of the magnetoshell interaction with neutral atmosphere in a spacecraft-fixed frame.

TABLE OF CONTENTS

1. INTRODUCTION.....	1
2. CONTROL VOLUME MODEL	2
3. OPERATING CONDITIONS	6
4. RESULTS AND DISCUSSION.....	6
5. CONCLUSION	8
APPENDICES.....	9
A. DEFINITION OF TERMS	9
ACKNOWLEDGMENTS	9
REFERENCES	9
BIOGRAPHY	10

1. INTRODUCTION

Aerocapture is an orbit insertion maneuver that uses drag of a planetary atmosphere on a spacecraft to transfer it from a hyperbolic trajectory to a closed elliptic orbit. Hall et al. [1] have determined that this maneuver yields a large advantage in cost and delivered mass to all eight solar system destinations with significant atmospheres. They also identify it as an enabling technology for otherwise infeasible missions to Jupiter, Saturn, and Neptune. Several relatively mature aerocapture technologies are under development, such as the Hypersonic Inflatable Aerodynamic Decelerator (HIAD) [2], the Adaptive Deployable Placement Technology (ADEPT) [3], and ballutes [4], yet none has ever been used on a mission because of the associated risks. Current aerocapture devices

rely on solid structures to deflect atmospheric flow and are therefore susceptible to the high heat and dynamic pressure inherent to reentry conditions. Plasma aerocapture is a proposed technology [5] to generate drag through interaction of the atmosphere with a plasma whose size and density can be modulated. This plasma, called a “magnetoshell,” can create a much larger drag area than most rigid aeroshells, allowing it to attain the same drag at higher altitudes and lower dynamic pressures. The proposed ability to modulate drag by controlling magnetic field strength also provides a mechanism for robust control of aerocapture maneuvers, potentially offering vast improvements over the accuracy of target orbits achieved compared to rigid devices.

Magnetoshells are created by injecting and confining plasma in a dipole magnetic field. Although some seed plasma is injected, the flow contributes overwhelmingly to sustaining the magnetoshell. The primary interactions of this plasma with the neutral atmosphere are charge exchange and electron-impact ionization. To see how this produces drag, let us observe a charge exchange interaction in a frame moving with the magnetoshell such that the plasma is stationary and neutrals stream in unidirectionally at orbital velocity (Figure 1).

The magnetic field contains a toroidal region of plasma which is encountered by a neutral particle with a large directional kinetic energy. The neutral undergoes charge exchange with an ion of some small, randomly directed energy. Because charge exchange conserves particle energy, this thermal ion becomes a thermal neutral and diffuses out of the system, no longer confined by magnetic forces. The original neutral, however, becomes a high-energy ion that is turned and trapped by the magnetic field through the Lorentz force. This turning is responsible for imparting the momentum of the atmospheric particle to the magnet and, subsequently, to the spacecraft itself. Though each individual particle produces a minuscule force, the production of new ions from the stream is so widespread that large macroscopic drag can occur. In fact, the effective drag surface of the magnetoshell can have a diameter several times the size of the magnet.

The plasma aerocapture concept was first proposed by Slough [5] as a high-plasma-beta, rotating magnetic field dipole towed behind a spacecraft like a “plasma parachute.” Kirtley [6] furthered its development by conceptualizing a simple electromagnet dipole containing a low-beta plasma, easing both energy requirements and engineering complexity. His work also derived the first analytical model of magnetoshell performance in aerocapture environments. This model was applied to prove the feasibility of using plasma aerocapture for the Human Mars DRA 5.0 cargo payloads [7] and a Neptune orbiter mission [8], in both cases indicating substantial improvements in mission cost and delivered mass over their proposed traditional aerocapture devices. Kirtley also performed the first two technology demonstrations. In the first [6], a small magnetoshell generated significant drag while attached to a thrust stand with an impinging plasma/neutral flow of around 1 km/s. The second demonstration [9] proved the feasibility of using an RF plasma source injected at center-field to seed the magnetoshell plasma. Hancock [10] performed an additional system analysis using Kirtley’s analytical model, finding that the magnet and power system are the most significant drivers of spacecraft mass. He also developed a trajectory simulation showing that a fixed-area maneuver is highly sensitive to the altitude at which the magnetoshell is activated, indicating that a higher-fidelity physical model enabling drag modulation is needed.

Despite these research efforts, there has not been a full system validation or self-consistent model verifying the feasibility of a magnetoshell spacecraft system. Ground testing this large-scale device in a low density, high velocity flow that simulates atmospheric entry is not possible in existing wind tunnels. Therefore, novel experimental techniques and simulation approaches must be developed. This paper details an analytical control volume model of the interaction between the plasma and the atmosphere during an aerocapture pass. The model is used for a parametric analysis of the effects of stream density, stream velocity, magnetic field strength, magnet size, and injected power/mass of seed plasma on the magnetoshell’s consumption of atmospheric energy and mass. As a technology that hinges on in-situ resource utilization (ISRU), analyzing its efficacy at leveraging the atmospheric flow will inform critical questions surrounding operational regimes and engineering requirements. Such questions bear on structural mass, propellant mass, and overall system power, all crucial to determining whether plasma aerocapture is feasible for modern spaceflight. Addressing them will ultimately enable direct comparison of magnetoshell performance to rigid aeroshells and propulsive orbit insertion. As the first self-consistent analysis of energy and mass utilization by the magnetoshell plasma, this model is a powerful new tool in the

overall effort to demonstrate feasibility and design missions with this technology.

The following is a brief summary of the work. An appropriate control volume is defined by characterizing the region of ion trapping by the dipole magnetic field. Equations of continuity and state are developed to capture the most important interactions between ions, electrons, stream neutrals, and magnetoshell (or “secondary”) neutrals. These equations are solved numerically over a wide range of spacecraft and atmospheric conditions to analyze scaling of energy and mass consumption with those parameters.

2. CONTROL VOLUME MODEL

Defining the Control Volume

In order to assess energy and mass consumption by the plasma, an appropriate volume must be identified to describe the physical extent of its interaction with the atmosphere. The mechanism of capturing particles relies on converting stream neutrals to ions while they are within the magnetic field’s grasp. Thus, a logical description of the plasma volume is the region inside which newly-formed ions from the stream remain trapped along field lines. We develop a particle trajectory solver to reveal this geometry of ion confinement. Although higher-order effects are included in the control volume model, single-particle analysis suffices to initially determine this boundary.

The equation of motion for an ion in a magnetic field is

$$\frac{d^2 \mathbf{x}}{dt^2} = \frac{q_i}{m_i} \frac{d\mathbf{x}}{dt} \times \mathbf{B} \quad (1)$$

where \mathbf{x} is the position vector, t is time, q_i is ion charge, m_i is ion mass, and \mathbf{B} is the magnetic field vector. The righthand side is the Lorentz force and no other forces on the particle are considered. We model the magnetoshell’s magnetic field as that of a loop of current centered at the origin with radius a in cylindrical coordinates (r, θ, z) . This is described as [11]

$$\mathbf{B} = \frac{1}{r} \hat{\boldsymbol{\theta}} \times \nabla \psi \quad (2)$$

$$\psi = \frac{2B_0 a^2 r (2 - k^2) K(k^2) - 2E(k^2)}{\pi k^2 \sqrt{(a+r)^2 + z^2}} \quad (3)$$

$$k^2 = \frac{4ra}{(r+a)^2 + z^2} \quad (4)$$

where $\hat{\boldsymbol{\theta}}$ is the azimuthal unit vector, ψ is the magnetic scalar flux function, K and E are complete elliptic integrals of the first and second kind respectively, and k is a substitute variable.

Equation (1) is normalized with $\hat{\mathbf{x}} = \mathbf{x}/r_c$, $\tau = tu_{sn}/r_c$, and $\hat{\mathbf{B}} = \mathbf{B}/B_0$ for magnet coil radius r_c , stream velocity u_{sn} , and center-field strength B_0 . The normalized equation of motion is

$$\frac{d^2 \hat{\mathbf{x}}}{d\tau^2} = \frac{1}{\rho_L} \frac{d\hat{\mathbf{x}}}{d\tau} \times \hat{\mathbf{B}} \quad (5)$$

where $\rho_L = r_L/r_c$ is the normalized ion Larmor radius. Equation (5) is used to track the 3D trajectories of ions seeded at gridded points in a 2D cross-section of the magnetic field. To simulate post-charge-exchange ions, the initial velocity of each particle is the stream velocity. Each trajectory is

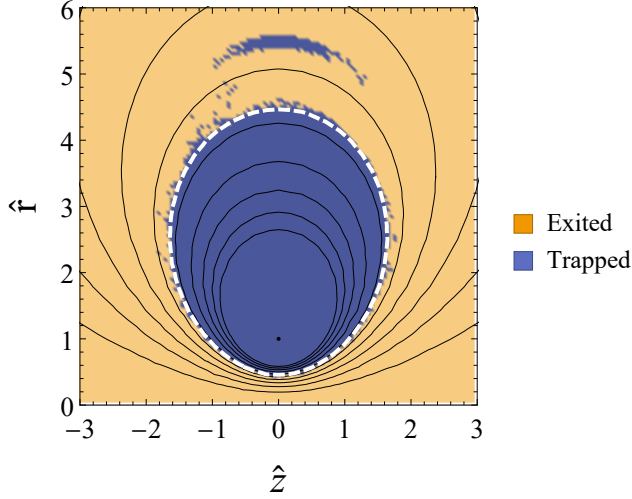


Figure 2. Single-particle analysis of ion trapping by the dipole magnetic field, shown in cross section cylindrical coordinates. The white dashed line is the $\psi^* = \sqrt{2\rho_L}$ contour. The point at (0,1) is the magnet coil.

propagated to $\tau = 100$. If the magnitude of $\hat{\mathbf{x}}$ exceeds 10 during that time, the particle is considered to have left the system; this is the criterion determining whether an ion is trapped or not.

The results of this analysis are shown in Figure 2. There is a clear spatial dependence on particle trapping that matches contours of the magnetic flux. We find the boundary of ion confinement to be the contour at $\psi^* = \sqrt{2\rho_L}$, forming a toroidal control volume. An anomalous ring of confined ions is observed with a radius larger than the toroid; this region is ignored for the purposes of this analysis.

Control Volume Equations

The interactions among magnetoshell plasma and atmospheric stream neutrals can be described by equations of continuity and state. In this system, three distinct species are tracked: ions (i), electrons (e), and “secondary” neutrals (2n). Secondary neutrals are those that result from collisions as opposed to stream neutrals (sn) that enter the control volume from the atmosphere. Explicit momentum equations for these three species are neglected. Instead, we close the equations using Fick’s Law to describe diffusion of mass and energy.

Continuity—The general form of the continuity equations is

$$\frac{\partial n_\alpha}{\partial t} + \nabla \cdot (n_\alpha \mathbf{u}_\alpha) = \sum \frac{\partial n_\alpha}{\partial t} \Big|_S \quad (6)$$

where n_α is the number density of species α and the righthand side is the sum of all sources and sinks S in species α . Equation (6) is normalized and integrated over the volume to obtain the continuity equations used in this model. The normalized species density is $\hat{n}_\alpha = n_\alpha/n_{\text{sn}}$ where n_{sn} is the stream density. The model equations take a final form of

$$\frac{d\hat{N}_\alpha}{d\tau} = \frac{d\hat{N}_\alpha}{d\tau} \Big|_{\text{diff}} + \sum \frac{d\hat{N}_\alpha}{d\tau} \Big|_S \quad (7)$$

where $\hat{N}_\alpha = \int \hat{n}_\alpha d\hat{V}$ is the normalized density integrated over the volume in normal coordinates $\hat{V} = V/r_c^3$. The first

term on the righthand side represents particle loss to diffusion and its particular form is derived later in this section.

Energy—The general form of the energy equations is

$$\frac{\partial \varepsilon_\alpha}{\partial t} + \nabla \cdot (\varepsilon_\alpha \mathbf{u}_\alpha) = \sum \frac{\partial \varepsilon_\alpha}{\partial t} \Big|_S \quad (8)$$

where $\varepsilon_\alpha = \frac{1}{2}m_\alpha n_\alpha u_\alpha^2 + p_\alpha/(\gamma - 1)$ is the total fluid energy density of species α as given by Meier and Shumlak [12] for particle mass m_α , fluid speed u_α , species pressure p_α , and specific heat ratio γ . Assuming ideal gases, $p_\alpha = n_\alpha k T_\alpha$, the lefthand side of Equation (8) can be written

$$\frac{\partial \varepsilon_\alpha}{\partial t} = \frac{\partial}{\partial t} \left(\frac{n_\alpha k T_\alpha}{\gamma - 1} \right) = \frac{k}{\gamma - 1} \left(\frac{\partial n_\alpha}{\partial t} T_\alpha + n_\alpha \frac{\partial T_\alpha}{\partial t} \right) \quad (9)$$

where k is the Boltzmann constant and T_α is the temperature of species α . Equation (9) is normalized with $\hat{T}_\alpha = T_\alpha/T_{\text{sn}}$ and $\hat{\varepsilon}_\alpha = \varepsilon_\alpha/\varepsilon_{\text{sn}}$ where $\varepsilon_{\text{sn}} \approx \frac{1}{2}m_{\text{sn}}n_{\text{sn}}u_{\text{sn}}^2$ is the stream energy density and $T_{\text{sn}} = m_{\text{sn}}u_{\text{sn}}^2/3k$ is the stream effective temperature for stream neutral mass m_{sn} . We neglect the pressure term in ε_{sn} by assuming the flow velocity is much higher than the acoustic velocity. After normalization and integrating over the control volume, the energy equations have the form

$$\begin{aligned} \frac{d\hat{E}_\alpha}{d\tau} &= \frac{2/3}{\gamma - 1} \left(\frac{d\hat{N}_\alpha}{d\tau} \hat{T}_\alpha + \hat{N}_\alpha \frac{d\hat{T}_\alpha}{d\tau} \right) \\ &= \frac{d\hat{E}_\alpha}{d\tau} \Big|_{\text{diff}} + \sum \frac{d\hat{E}_\alpha}{d\tau} \Big|_S \end{aligned} \quad (10)$$

where $\hat{E}_\alpha = \int \hat{\varepsilon}_{\text{sn}} d\hat{V}$ is the total energy of α -species particles in the control volume.

Plasma Model Equations

Equations (7) and (10) are used to develop evolutions of energy and mass for the three tracked species (i, e, and 2n). Five equations are necessary,

1. Ion/electron continuity equation
2. Secondary neutral continuity equation
3. Ion equation of state
4. Electron equation of state
5. Secondary neutral equation of state

to track the five relevant quantities,

1. Ion population \hat{N}_i
2. Secondary neutral population \hat{N}_{2n}
3. Ion temperature \hat{T}_i
4. Electron temperature \hat{T}_e
5. Secondary neutral temperature \hat{T}_{2n}

We assume the plasma is quasineutral with singly charged ions, allowing $\hat{N}_i = \hat{N}_e$ and just one continuity equation to describe both ions and electrons. To get from Equations (7) and (10) to these five equations, all contributing factors to energy and mass in the plasma volume are carefully considered. These contributions are converted into normalized, volume-averaged terms that are summed as indicated by the righthand sides of Equations (7) and (10).

To derive these contributing terms, approximations to the geometry and physics of the system must be made. The plasma is assumed to be low-beta and therefore adhere strongly to field lines. This allows us to set the plasma density profile equal to a scaled value of the magnetic field profile, $\hat{n}_\alpha(\mathbf{x}) = \hat{n}_{\alpha,0} \hat{B}(\mathbf{x})$, where $\hat{n}_{\alpha,0}$ is the normalized center-field density of charged species α . For simplicity, this assumption is extended to the secondary neutrals as well, since these particles are borne from the plasma. By integrating over the control volume, the center-field densities can be rewritten as $\hat{n}_{\alpha,0} = \hat{N}_\alpha / \int \hat{B} d\hat{V}$. Computational load is eased by simplifying gradients and divergences to $1/r_c$.

Diffusion—The diffusive term in Equation (6) must be developed into nondimensional volume-averaged form. Using Fick's Law,

$$n_\alpha \mathbf{u}_\alpha = -D \nabla n_\alpha \quad (11)$$

where D is the diffusion coefficient, we may derive an expression for $\frac{\partial \hat{N}_\alpha}{\partial \tau} \Big|_{\text{diff}}$ to use in continuity and energy balance. Since D can have different spatial dependencies in different models of diffusion, the cases of ions/electrons and secondary neutrals are treated separately.

The ion/electron continuity equation incorporates several diffusion models in sum. The diffusive term is

$$\frac{\partial n_i}{\partial \tau} = \nabla \cdot (n_i \mathbf{u}_i) = -\nabla \cdot [(D_B + D_c) \nabla n_i] \quad (12)$$

where D_B is the anomalous Bohm diffusion coefficient and D_c is the coefficient of diffusion due to electron-ion and electron-neutral collisions. We carry out the derivation for ion diffusion which is identical to electron diffusion due to ambipolar effects. D_B is described by Lieberman [13] while D_c is given by a combination of coefficients from Goldston [14]:

$$D_B = \frac{kT_e}{16eB} \quad (13)$$

$$D_c = \frac{m_e(\nu_{ei} + \nu_{en})}{e^2 B^2} k(T_e + T_i) \quad (14)$$

where e is the elementary charge, $B = |\mathbf{B}|$, and ν_{ei} and ν_{en} are electron-ion and electron-neutral collision frequencies respectively. Note that $D_B \propto 1/B$ while $D_c \propto 1/B^2$, thus integrating over the control volume yields two diffusion terms. The same normalization scheme is applied as before and the divergence theorem allows us to convert the volume integrals to surface integrals, giving

$$\frac{d\hat{N}_i}{d\tau} \Big|_{\text{diff}} = -\hat{D}_B \hat{T}_e \hat{N}_i \frac{I_{\text{diff}}}{I_B} - \hat{D}_c (\hat{T}_e + \hat{T}_i) \hat{N}_i \frac{I_c}{I_B} \quad (15)$$

where \hat{D}_B and \hat{D}_c are normalized forms of D_B and D_c respectively and I_{diff} , I_B , and I_c are surface integrals resulting from the derivation; these parameters are defined in Appendix A.

Secondary neutral diffusion is treated by considering momentum-transfer collisions with ions and gas-kinetic collisions with other secondary neutrals. A general diffusion coefficient is given by Lieberman [13] and we adapt it for collisions with two species,

$$D_{2n} = \frac{2kT_{2n}}{m_{2n}(n_i \sigma_{Qm} + n_{2n} \sigma_{gk})} \left(\frac{16kT_{2n}}{\pi m_{2n}} \right)^{-1/2} \quad (16)$$

where σ_{Qm} is the momentum-transfer cross section between ions and neutrals and σ_{gk} is the gas-kinetic cross section of mutual secondary neutral collisions. Our assumption of low plasma beta, $n_\alpha \propto B$, gives a scaling of $D_{2n} \propto 1/B$. After normalization, integrating over the volume, and applying the divergence theorem, the secondary neutral diffusive term is

$$\frac{d\hat{N}_{2n}}{d\tau} \Big|_{\text{diff}} = -\hat{D}_{2n} \sqrt{\hat{T}_{2n}} \hat{N}_{2n} I_{\text{diff}} \quad (17)$$

where \hat{D}_{2n} is a normalized form of D_{2n} , defined in Appendix A. Because of the same $1/B$ scaling, the surface integral I_{diff} is identical to that in the Bohm diffusion term (15).

Energy diffusion is derived simply from the particle diffusion described above. Assuming the fluid velocity is much smaller than the acoustic velocity, $\varepsilon_\alpha \approx p/(\gamma - 1)$, and that T_α is uniform, the convective term in Equation (8) becomes

$$\nabla \cdot (\varepsilon_\alpha \mathbf{u}_\alpha) = \frac{kT_\alpha}{\gamma - 1} \nabla \cdot (n_\alpha \mathbf{u}_\alpha) \quad (18)$$

Fick's Law can be applied to this identically as in Equation (12), ultimately yielding an energy diffusion term that is the product of the continuity term and a normalized energy:

$$\frac{d\hat{E}_\alpha}{d\tau} \Big|_{\text{diff}} = -\frac{d\hat{N}_\alpha}{d\tau} \Big|_{\text{diff}} \frac{2/3}{\gamma - 1} \hat{T}_\alpha \quad (19)$$

Ion/Electron Continuity—The following sources and sinks are included in the continuity equation for ions and electrons, listed in alphabetical order of the subscripts used to describe them:

- diff: ion/electron diffusion
- inj: plasma injection from the spacecraft
- iz,2n: ionization of secondary neutrals
- iz,sn: ionization of stream neutrals

Note that charge exchange makes no net contribution to the ion population since it simultaneously produces and removes an ion. The full form of the ion/electron continuity equation is

$$\begin{aligned} \frac{d\hat{N}_i}{d\tau} = & - \underbrace{\hat{D}_B \hat{T}_e \hat{N}_i \frac{I_{\text{diff}}}{I_B}}_{\text{Bohm diff}} - \underbrace{\hat{D}_c (\hat{T}_e + \hat{T}_i) \hat{N}_i \frac{I_c}{I_B}}_{\text{coll. diff}} \\ & + \underbrace{\hat{N}_{\text{inj}}}_{\text{inj}} + \underbrace{X_{\text{iz},2n} \hat{N}_e \hat{N}_{2n} \frac{I_{B2}}{I_B^2}}_{\text{iz,2n}} + \underbrace{X_{\text{iz,sn}} \hat{N}_e \frac{I_{\text{sn}}}{I_B}}_{\text{iz,sn}} \end{aligned} \quad (20)$$

$\hat{N}_{\text{inj}} = \frac{\dot{n}_{\text{inj}}}{m_i n_{\text{sn}} u_{\text{sn}} r_c^2}$ is the normalized particle injection rate from seeding plasma. \hat{D}_B , \hat{D}_c , X_{reac} , and the integrals I_{diff} , I_c , I_B , I_{B2} , and I_{sn} that result from spatial averaging are defined in Appendix A.

Secondary Neutral Continuity—The following sources and sinks are included in the continuity equation for secondary neutrals, listed in alphabetical order of the subscripts used to describe them:

- cx,sn: charge exchange between stream neutrals and ions
- diff: neutral diffusion

- iz,2n: ionization of secondary neutrals

Charge exchange contributes to the secondary neutral population when an ion loses its charge to a stream neutral. The full form of the secondary neutral continuity equation is

$$\frac{d\hat{N}_{2n}}{d\tau} = \underbrace{X_{cx,sn}\hat{N}_e\frac{I_{sn}}{I_B}}_{cx,sn} - \underbrace{\hat{D}_{2n}\sqrt{\hat{T}_{2n}}\hat{N}_{2n}I_{diff}}_{diff} - \underbrace{X_{iz,2n}\hat{N}_e\hat{N}_{2n}\frac{I_{B2}}{I_B^2}}_{iz,2n} \quad (21)$$

\hat{D}_{2n} is defined in Appendix A.

Ion Energy—The following sources and sinks are included in the equation of state for ions, listed in alphabetical order of the subscripts used to describe them:

- cx,2n: charge exchange between secondary neutrals and ions
- cx,sn: charge exchange between stream neutrals and ions
- diff: ion diffusion
- inj: plasma injection from the spacecraft
- iz,2n: ionization of secondary neutrals
- iz,sn: ionization of stream neutrals
- th,ie: thermalization between ions and electrons

The charge exchange and ionization terms are derived from Meier and Shumlak's plasma/neutral model [12]. Thermalization is modeled according to Braginskii's transport equations [15]. The full form of the ion energy equation is

$$\begin{aligned} \frac{d\hat{E}_i}{d\tau} = & \frac{2/3}{\gamma-1} \left(\frac{d\hat{N}_i}{d\tau}\hat{T}_i + \hat{N}_i\frac{d\hat{T}_i}{d\tau} \right) = \\ & \underbrace{\frac{3}{2}Z_{cx,2n}(\hat{v}_{T,2n}^2V_{i,2n} - \hat{v}_{T,i}^2V_{2n,i})\hat{N}_i\hat{N}_{2n}\frac{I_{B2}}{I_B^2}}_{cx,2n} \\ & + \underbrace{M_{i/sn} \left(X_{cx,sn}\hat{N}_e - \frac{3}{2}Z_{cx,sn}\hat{N}_i\hat{v}_{T,i}^2\sqrt{\frac{64}{9\pi}\hat{v}_{T,i}^2+1} \right) \frac{I_{sn}}{I_B}}_{cx,sn} \\ & - \underbrace{\frac{2/3}{\gamma-1} \left(\hat{D}_B\hat{T}_e\hat{N}_i\frac{I_{diff}}{I_B} + \hat{D}_c(\hat{T}_e + \hat{T}_i)\hat{N}_i\frac{I_c}{I_B} \right) \hat{T}_i}_{diff} \\ & + \underbrace{f_i\hat{P}_{inj}}_{inj} + \underbrace{X_{iz,2n}\hat{N}_e\hat{N}_{2n}\hat{T}_{2n}\frac{I_{B2}}{I_B^2}}_{iz,2n} \\ & + \underbrace{M_{i/sn}X_{iz,sn}\hat{N}_e\frac{I_{sn}}{I_B}}_{iz,sn} + \underbrace{\frac{2M_{efi}}{\tau_e}\hat{N}_i(\hat{T}_e - \hat{T}_i)}_{th,ie} \quad (22) \end{aligned}$$

$\hat{v}_{T,\alpha} = \sqrt{2kT_\alpha/m_\alpha/u_{sn}}$ is the normalized thermal velocity of species α . $M_{\alpha/\beta} = m_\alpha/m_\beta$ is the ratio of particle masses of species α and β . $\hat{P}_{inj} = \frac{r_c}{\varepsilon_{sn}u_{sn}}P_{inj}$ is the normalized injected power P_{inj} of seeded plasma, while $f_i \in [0, 1]$ is the fraction of power coupled to ions in the plasma source. $\tau_e = t_e u_{sn}/r_c$ is the normalized version of the electron thermalization time t_e given by Braginskii [15]. Z_{reac} and $V_{\alpha,\beta}$ are defined in Appendix A.

Electron Energy—The following sources and sinks are included in the equation of state for electrons, listed in alphabetical order of the subscripts used to describe them:

- diff: electron diffusion
- inj: spacecraft plasma injection
- iz,2n: ionization of secondary neutrals
- iz,sn: ionization of stream neutrals
- th,ie: thermalization between ions and electrons

Thermalization is modeled as in the ion energy equation. Ionizations of secondary and stream neutrals are derived from Meier and Shumlak [12]. The full form of the electron energy equation is

$$\begin{aligned} \frac{d\hat{E}_e}{d\tau} = & \frac{2/3}{\gamma-1} \left(\frac{d\hat{N}_i}{d\tau}\hat{T}_e + \hat{N}_i\frac{d\hat{T}_e}{d\tau} \right) = \\ & - \underbrace{\frac{2/3}{\gamma-1} \left(\hat{D}_B\hat{T}_e\hat{N}_i\frac{I_{diff}}{I_B} + \hat{D}_c(\hat{T}_e + \hat{T}_i)\hat{N}_i\frac{I_c}{I_B} \right) \hat{T}_e}_{diff} \\ & \underbrace{(1-f_i)\hat{P}_{inj}}_{inj} + \underbrace{X_{iz,2n}\hat{N}_e\hat{N}_{2n} \left(M_{e/2n}\hat{T}_{2n} - \frac{2}{3}\hat{T}_{iz,2n} \right) \frac{I_{B2}}{I_B^2}}_{iz,2n} \\ & + \underbrace{\left(M_{e/sn} - \frac{2}{3}\hat{T}_{iz,sn} \right) X_{iz,sn}\hat{N}_e\frac{I_{sn}}{I_B}}_{iz,sn} - \underbrace{\frac{2M_{efi}}{\tau_e}\hat{N}_i(\hat{T}_e - \hat{T}_i)}_{th,ie} \quad (23) \end{aligned}$$

$\hat{T}_{iz,\alpha} = U_{iz,\alpha}/kT_{sn}$ is the normalized electron-impact ionization energy $U_{iz,\alpha}$ of neutral species α .

Secondary Neutral Energy—The following sources and sinks are included in the equation of state for secondary neutrals, listed in alphabetical order of the subscripts used to describe them:

- cx,2n: charge exchange between secondary neutrals and ions
- cx,sn: charge exchange between stream neutrals and ions
- diff: diffusion of secondary neutrals
- iz,2n: ionization of secondary neutrals

The charge exchange and ionization terms are derived from Meier and Shumlak [12]. The full form of the secondary neutral energy equation is

$$\begin{aligned} \frac{d\hat{E}_{2n}}{d\tau} = & \frac{2/3}{\gamma-1} \left(\frac{d\hat{N}_{2n}}{d\tau}\hat{T}_{2n} + \hat{N}_{2n}\frac{d\hat{T}_{2n}}{d\tau} \right) = \\ & - \underbrace{\frac{3}{2}Z_{cx,2n}(\hat{v}_{T,2n}^2V_{i,2n} - \hat{v}_{T,i}^2V_{2n,i})\hat{N}_i\hat{N}_{2n}\frac{I_{B2}}{I_B^2}}_{cx,2n} \\ & + \underbrace{\frac{3}{2}M_{i/sn}Z_{cx,sn}\hat{N}_i \left(\hat{v}_{T,i}^2\sqrt{\frac{64}{9\pi}\hat{v}_{T,i}^2+1} \right) \frac{I_{sn}}{I_B}}_{cx,sn} \\ & - \underbrace{\frac{2/3}{\gamma-1}\hat{D}_{2n}\hat{N}_{2n}\hat{T}_{2n}^{3/2}I_{diff}}_{diff} - \underbrace{X_{iz,2n}\hat{N}_e\hat{N}_{2n}\hat{T}_{2n}\frac{I_{B2}}{I_B^2}}_{iz,2n} \quad (24) \end{aligned}$$

The terms in this equation are common to the preceding equations and definitions are found in Appendix A.

3. OPERATING CONDITIONS

Input Parameters

The control volume equations (20) to (24) constitute a system of five nonlinear ODEs in five variables. The magnetoshell plasma is simulated by propagating these equations using a numerical solver from which the solutions of $\hat{N}_i(\tau)$, $\hat{N}_{2n}(\tau)$, $\hat{T}_i(\tau)$, $\hat{T}_e(\tau)$, and $\hat{T}_{2n}(\tau)$ are output. Each simulation of a single combination of operating conditions takes roughly 15 seconds to solve on a modern desktop computer. A matrix of input parameters yields results across a variety of potential magnetoshell and environmental conditions. The variables examined are stream density n_{sn} , stream speed u_{sn} , magnetic field strength B_0 , magnet size r_c , plasma injection mass flow rate \dot{m}_{inj} , and plasma injection power P_{inj} . The ranges of input parameters used are given in Table 1. We propagate the equations to $\tau = 3 \times 10^4$ to ensure a steady state of populations and temperatures is reached. The results derived from these simulations come from the final steady state values of the output variables.

Table 1. Input ranges of the six variable parameters.

Parameter	Min	Max	Units
n_{sn}	10^{16}	10^{18}	m^{-3}
u_{sn}	2	20	km/s
B_0	0.01	1	T
r_c	0.25	2	m
\dot{m}_{inj}	0.03	10	mg/s
P_{inj}	0	1000	W

Plasma Properties

Argon is used as the plasma and stream species; though this does not represent any known atmospheric entry, it is used in this study to simplify the physical interactions and reveal crucial scaling relations. We assume a value of $\gamma = 5/3$. The Ar-Ar⁺ momentum transfer cross section $\sigma_{Qm,Ar}$ and charge exchange cross section $\sigma_{cx,Ar}$ are tabulated by Phelps [16]. The Ar-Ar gas kinetic cross section $\sigma_{gk,Ar}$ is published by Lieberman [13] via Smirnov [17]. An analytical form found in Chapter 11 of Goldston [14] is used to compute the electron-ion collision frequency for Argon $\nu_{ei,Ar}$. The electron-neutral collision frequency for Argon $\nu_{en,Ar}$ is modeled after Itikawa [18] using data from Harstad [19]. The electron-impact ionization rate coefficient for Argon $R_{iz,Ar}$ is taken from the NRL Plasma Formulary [20]. In all simulated cases, $f_i = 0.5$ for equal heating of ions and electrons by the seed plasma injector.

4. RESULTS AND DISCUSSION

In order to operate the magnetoshell, some plasma seeding is typically required. One measure of the device's ISRU effectiveness is the return on mass and power injection; that is, how much mass and energy is absorbed from the atmosphere compared to the amount supplied by the spacecraft. If the magnetoshell is able to utilize a large amount of atmospheric mass and energy, there is good indication of benefits over thrusters which can only produce forces from stored mass and energy. This can also be compared directly with rigid

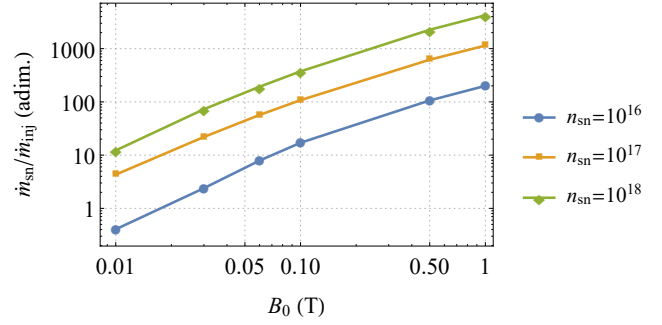


Figure 3. Atmospheric density n_{sn} and magnetic field strength B_0 both have a positive effect on the rate of mass capture from the atmosphere \dot{m}_{sn} . Ambient conditions: $u_{sn} = 8$ km/s; $r_c = 1$ m; $\dot{m}_{inj} = 1$ mg/s; $P_{inj} = 300$ W.

aerocapture concepts which absorb or deflect all the energy and mass incident on their surface. We therefore focus our discussion on absorbed energy and mass as well as the return on injected power and propellant across different ambient parameters. Though drag estimates could be made based on absorbed mass, there are more complex magnetic effects reaching far outside the control volume that impact the actual drag force generated. For this reason, we leave discussions of drag for future studies.

Figure 3 shows the relationship between applied magnetic field strength, B_0 , and the rate of mass ingestion by the plasma from the atmosphere, \dot{m}_{sn} . The operating conditions are $u_{sn} = 8$ km/s, $r_c = 1$ m, $\dot{m}_{inj} = 1$ mg/s, and $P_{inj} = 300$ W. These are reasonable values for a magnetoshell system at no extreme of environmental or engineering constraints. The ingested mass is computed from the sum of the ionization and charge exchange terms converting stream neutrals to ions. We clearly see a positive effect of both field strength and stream density on ingested mass. At low densities, the ingested mass can be very little without enough magnetic confinement, likely restricting the operational regime. At the other extreme, however, the plasma captures 4,000 times more mass from the flow than the amount injected. This result bodes well for the notion of drag modulation through control of the magnetic field strength [5]. Another key takeaway is that the ingested mass correlates directly with stream density. In practice, this means the magnetoshell drag force may be predictable like that of solid decelerators which are described by

$$F_D = \frac{1}{2} C_D m_{sn} n_{sn} A u_{sn}^2 \quad (25)$$

where F_D is the drag force, C_D is the coefficient of drag, and A is the cross-sectional area. Figure 3 implies that for a given operating state, an equation similar to (25) may describe magnetoshell drag.

Figure 4 shows a similar effect of field strength and stream density on ingested power, P_{sn} , for operating parameters of $u_{sn} = 8$ km/s, $r_c = 1$ m, and $\dot{m}_{inj} = 1$ mg/s. Notably, however, the input power in Figure 4 is $P_{inj} = 0$ W, demonstrating for the first time that the plasma can self-sustain with no onboard energy supply. At the upper extreme, the plasma is capable of absorbing over 100 kW of power from the flow, and even at moderate field strengths it can utilize several hundreds or thousands of watts.

Figure 5 shows the fraction η of flow energy and mass incident on the magnetoshell volume that is being absorbed

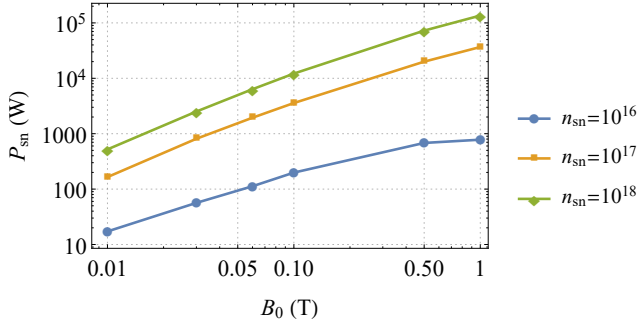


Figure 4. Stronger magnetic fields B_0 result in higher power absorbed from the atmosphere P_{sn} at all densities n_{sn} . Ambient conditions: $u_{\text{sn}} = 8$ km/s; $r_c = 1$ m; $\dot{m}_{\text{inj}} = 1$ mg/s; $P_{\text{inj}} = 0$ W.

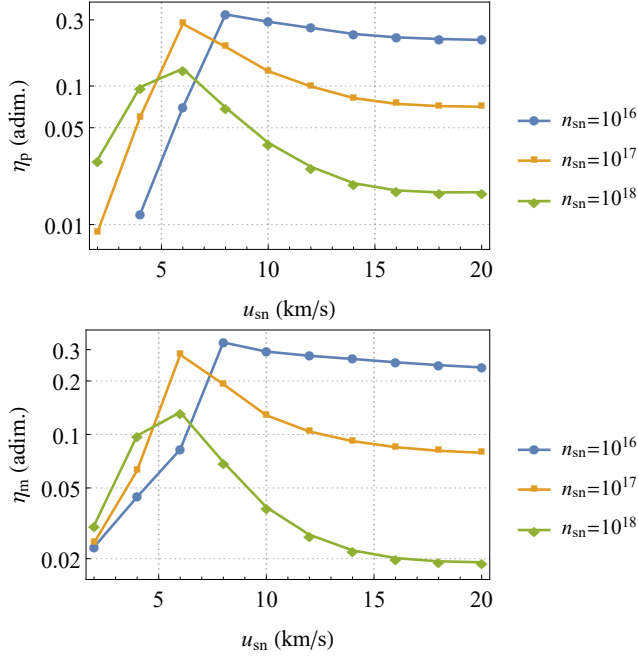


Figure 5. Utilization fraction η of atmospheric energy (top) and mass (bottom). Ambient conditions: $B_0 = 0.5$ T; $r_c = 1$ m; $\dot{m}_{\text{inj}} = 1$ mg/s; $P_{\text{inj}} = 300$ W.

by the plasma. Ambient conditions are $B_0 = 0.5$ T, $r_c = 1$ m, $\dot{m}_{\text{inj}} = 1$ mg/s, and $P_{\text{inj}} = 300$ W. This “utilization fraction” is defined for power as $\eta_p = P_{\text{sn}}/P_{\text{max}}$ where P_{sn} is the power absorbed by the plasma and P_{max} is the total incident power on the control volume. $\eta_m = \dot{m}_{\text{sn}}/\dot{m}_{\text{max}}$ is similarly defined for absorbed and total incident mass flow. The actual value of η ranges from a few percent up to around 1/3. It falls off dramatically at lower velocities as charge exchange interaction with the slower flow becomes very weak and cool electron temperatures limit ionization. The peak utilization fractions appear to occur in the 6–10 km/s velocity range, a regime of great interest for Earth return and Mars aerocapture applications. At these velocities, charge exchange swells to a maximum and the plasma is able to absorb a large fraction of flow. As the velocity increases, the charge exchange rate falls off while ionization rates increase to a steady maximum, causing the asymptotic behavior observed at the far right of the plots. This result is significant, as previous analyses of plasma aerocapture held

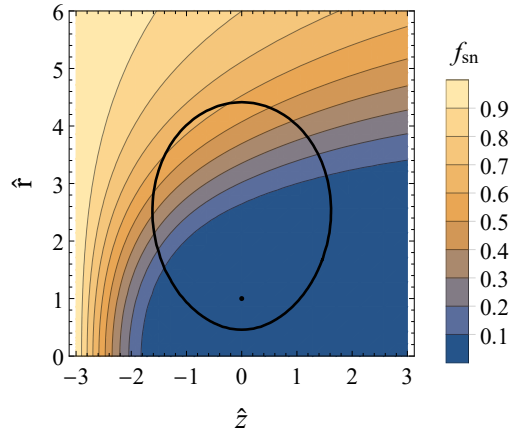


Figure 6. Fraction of stream neutrals untouched by the plasma. The control volume is marked by the black line. Ambient conditions: $n_{\text{sn}} = 10^{17}$ m $^{-3}$; $u_{\text{sn}} = 12$ km/s; $B_0 = 0.5$ T; $r_c = 1$ m; $\dot{m}_{\text{inj}} = 1$ mg/s; $P_{\text{inj}} = 300$ W.

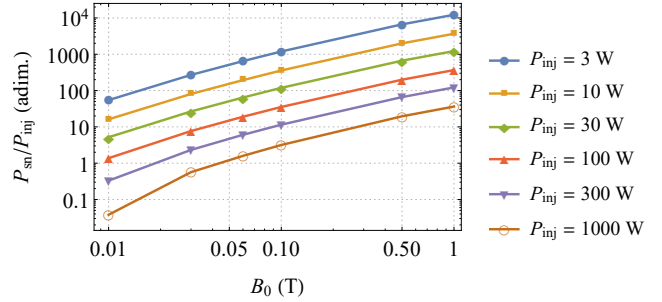


Figure 7. Return on input power is diminished as input power is increased. Ambient conditions: $n_{\text{sn}} = 10^{17}$ m $^{-3}$; $u_{\text{sn}} = 8$ km/s; $r_c = 1$ m; $\dot{m}_{\text{inj}} = 1$ mg/s.

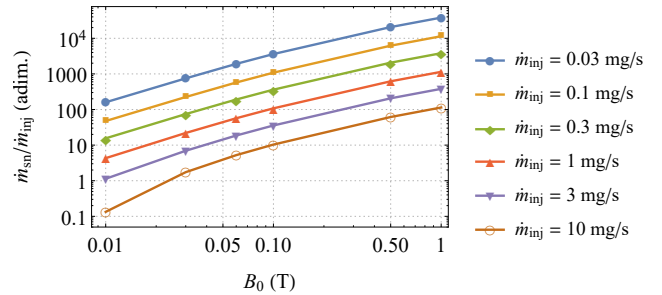


Figure 8. Return on mass injected is diminished as mass injection is increased. Ambient conditions: $n_{\text{sn}} = 10^{17}$ m $^{-3}$; $u_{\text{sn}} = 8$ km/s; $r_c = 1$ m; $\dot{m}_{\text{inj}} = 1$ mg/s.

the assumption that the magnetoshell was completely opaque to the flow. Figure 5 reveals that a certain amount of the stream instead passes through the plasma untouched. Figure 6 demonstrates this more visually, showing the spatial variation of a fraction $f_{\text{sn}} \in [0, 1]$ representing the portion of stream neutrals untouched by the plasma. In other words, low f_{sn} means the stream is highly utilized. We clearly see that there are portions of the control volume not fully blocking the flow. It is also clear that much of the interaction occurs outside the control volume; these particles are not trapped as defined by particle trajectory analysis but may contribute heavily to drag through magnetic deflection.

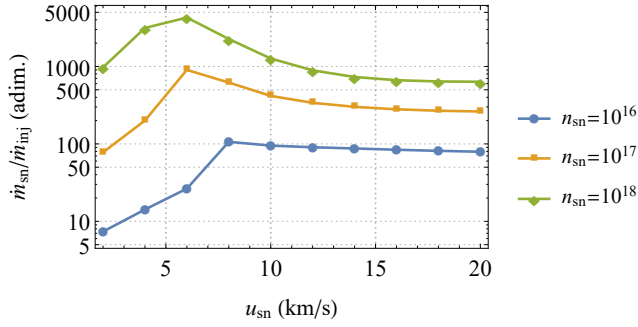


Figure 9. Mass ingestion is weakly negative with increasing stream velocity. Ambient conditions: $B_0 = 0.5$ T; $r_c = 1$ m; $\dot{m}_{inj} = 1$ mg/s; $P_{inj} = 300$ W.

Figure 7 reveals a diminishing return on input power, P_{sn}/P_{inj} , as input power is increased under constant operating conditions $n_{sn} = 10^{17} \text{ m}^{-3}$, $u_{sn} = 8$ km/s, $r_c = 1$ m, and $\dot{m}_{inj} = 1$ mg/s. This further confirms the finding that spacecraft power efficiency may be optimized by minimizing the onboard energy supply, since the plasma is self-sustaining from flow energy alone. The scaling is nearly identical for return on mass injection, $\dot{m}_{sn}/\dot{m}_{inj}$, as shown in Figure 8. However, we find that the plasma is unable to self-sustain when injected mass is brought to zero. This implies that some finite amount of fuel is required to operate the magnetoshell, and therefore some small power is needed to ionize the fuel. Even still, the propellant demand may be less than a gram total, since aerocapture maneuvers typically last just a few minutes and the necessary flow rate is less than 1 mg/s.

Both Figures 9 and 10 demonstrate the same dropoff at low velocities as that observed in Figure 5, again due to the drastic decrease in charge exchange reactions in that regime. At higher speeds, Figure 9 shows a weakly negative correlation between stream velocity and absorbed mass for $B_0 = 0.5$ T, $r_c = 1$ m, $\dot{m}_{inj} = 1$ mg/s, and $P_{inj} = 300$ W. On the contrary, Figure 10 demonstrates enhanced energy absorption as velocity increases. The discrepancy between these effects results from the particular dynamics of the magnetoshell. Recalling the control volume boundary $\psi^* = \sqrt{2\rho_L}$, we observe a decrease in the cross-sectional area A of the control volume with increasing velocity of about $A \propto 1/u_{sn}$. This happens to perfectly balance the increase in atmospheric mass flux, $m_{sn}n_{sn}u_{sn}$, and their combination yields a constant incident mass flow \dot{m}_{max} across all velocities. Thus the decreasing utilization of that mass, η_m , observed in Figure 5, produces the negative correlation in absorbed mass of Figure 9. However, the incident power scales more strongly with velocity, $P_{max} \propto u_{sn}^3$, overcoming the effect of the shrinking magnetoshell. The scaling of the power utilization fraction η_p is what gives Figure 10 its particular shape.

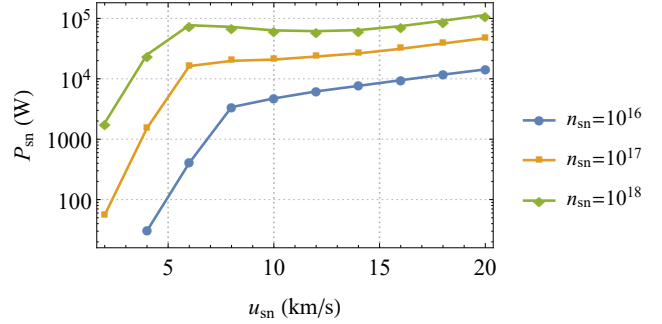


Figure 10. Ingested power increases at higher velocities. Ambient conditions: $B_0 = 0.5$ T; $r_c = 1$ m; $\dot{m}_{inj} = 1$ mg/s; $P_{inj} = 300$ W.

5. CONCLUSION

We present a novel analytical model of the interaction between a magnetoshell plasma and a hypersonic neutral flow. This model is applied to a parametric investigation of atmospheric mass and energy utilization during a plasma aerocapture maneuver. Some important results are revealed by this analysis. We find a strong impact of magnetic field strength on the absorption of power and mass from the flow. This confirms that the device drag can be modulated through power application to the magnet, as previous works have suggested. However, this is the first time this phenomenon is proven from a self-consistent model. Another long-standing suggestion confirmed by this model is that the plasma can self-sustain from flow energy alone with no strict onboard energy requirement. However, some mass injection is needed to sustain the plasma, though the amount is on the order of <1 gram over the course of a full maneuver. The fraction of flow utilized, η , is between 0.01–0.33 with optimal utilization occurring in regimes where charge exchange with the atmosphere is maximized. The finding that $\eta < 1$ challenges previous assumptions that the plasma fully blocks the flow. Finally, we find that the absorbed mass actually decreases with increasing spacecraft velocity due to the shrinking size of the magnetoshell and diminishing charge exchange contributions. The absorbed power still increases though, as its strong scaling with flow velocity overcomes these effects.

Ultimately, we desire to use this model in performance prediction and analysis of a plasma aerocapture spacecraft subsystem. Higher order effects must be considered to determine the actual drag produced, power required, overall mass, and flight envelopes of such a system. However, the results presented here are a significant step towards understanding the parameters governing magnetoshell performance. This model is a tool that may eventually be coupled with flight trajectory propagators to answer pressing questions of plasma aerocapture implementation.

APPENDICES

A. DEFINITION OF TERMS

Some terms referenced throughout the paper are found here in alphabetical order (with greek characters at the end). Note that $\hat{\nabla}$ is the gradient operator in normalized coordinates, $d\hat{S}$ is the differential surface element in normalized coordinates, \hat{z}' is a dummy variable, β is an arbitrary species, “*reac*” denotes an arbitrary reaction, and R_{reac} is the rate coefficient for the given reaction.

$$\begin{aligned} \hat{D}_{2n} &= \frac{\sqrt{\pi k T_{\text{sn}}/4m_{2n}}}{n_{\text{sn}} r_c u_{\text{sn}} (\hat{N}_i \sigma_{\text{Qm}} + \hat{N}_{2n} \sigma_{\text{gk}})} & \hat{D}_{\text{B}} &= \frac{k T_{\text{sn}}}{16e B_0 r_c u_{\text{sn}}} \\ \hat{D}_{\text{c}} &= \frac{m_e k T_{\text{sn}} (\nu_{\text{ei}} + \nu_{\text{en}})}{e^2 B_0^2 r_c u_{\text{sn}}} & \hat{E}_{\alpha} &= \int \hat{\varepsilon}_{\alpha} d\hat{V} \\ I_{\text{B}} &= \int \hat{B} d\hat{V} & I_{\text{B}2} &= \int \hat{B}^2 d\hat{V} \\ I_{\text{c}} &= \oint \frac{\hat{\nabla} \hat{B}}{\hat{B}^2} d\hat{S} & I_{\text{diff}} &= \oint \frac{\hat{\nabla} \hat{B}}{\hat{B}} d\hat{S} \\ I_{\text{sn}} &= \int \hat{B} \left(\exp \left[- \int_0^{\hat{z}'} \hat{B} d\hat{z}' \right] \right)^{(X_{\text{cx,sn}} + X_{\text{iz,sn}}) \hat{n}_{\text{e},0}} d\hat{V} \\ M_{\alpha/\beta} &= \frac{m_{\alpha}}{m_{\beta}} & \hat{n}_{\alpha,0} &= \frac{\hat{N}_{\alpha}}{\int \hat{B} d\hat{V}} \\ \hat{N}_{\text{inj}} &= \frac{\hat{m}_{\text{inj}}}{m_i n_{\text{sn}} u_{\text{sn}} r_c^2} & \hat{N}_{\alpha} &= \int \hat{n}_{\alpha} d\hat{V} \\ \hat{P}_{\text{inj}} &= \frac{r_c}{\varepsilon_{\text{sn}} u_{\text{sn}}} P_{\text{inj}} & \rho_{\text{L}} &= \frac{r_{\text{L}}}{r_c} \\ \hat{T}_{\text{iz},\alpha} &= \frac{U_{\text{iz},\alpha}}{k T_{\text{sn}}} & T_{\text{sn}} &= \frac{m_{\text{sn}} u_{\text{sn}}^2}{3k} \\ \hat{v}_{\text{T},\alpha} &= \frac{1}{u_{\text{sn}}} \sqrt{\frac{2k T_{\alpha}}{m_{\alpha}}} & V_{\alpha,\beta} &= \sqrt{\frac{4}{\pi} \hat{v}_{\text{T},\alpha}^2 + \frac{64}{9\pi} \hat{v}_{\text{T},\beta}^2} \\ X_{\text{reac}} &= \frac{R_{\text{reac}} n_{\text{sn}} r_c}{u_{\text{sn}}} & Z_{\text{reac}} &= n_{\text{sn}} r_c \sigma_{\text{reac}} \\ \varepsilon_{\text{sn}} &= \frac{1}{2} m_{\text{sn}} n_{\text{sn}} u_{\text{sn}}^2 & \tau_{\text{e}} &= \frac{t_{\text{e}} u_{\text{sn}}}{r_c} \end{aligned}$$

ACKNOWLEDGMENTS

This work was supported by a NASA Space Technology Research Fellowship. We thank Dr. Robert Moses at NASA Langley Research Center for his contributions to the development of this concept through conversations and reviews.

REFERENCES

- [1] J. L. Hall, M. A. Noca, and R. W. Bailey, “Cost-Benefit Analysis of the Aerocapture Mission Set,” *Journal of Spacecraft and Rockets*, vol. 42, no. 2, pp. 309–320, 2005. [Online]. Available: <http://arc.aiaa.org/doi/10.2514/1.4118>
- [2] S. J. Hughes, F. M. Cheatwood, A. M. Calomino, H. S. Wright, M. E. Wusk, and M. F. Hughes, “Hypersonic Inflatable Aerodynamic Decelerator (HIAD) Technology Development Overview,” NASA Langley Research Center, San Jose, CA, Tech. Rep., 2013. [Online]. Available: <http://arc.aiaa.org/doi/10.2514/6.2011-2524>
- [3] E. Venkatapathy, K. Hamm, I. Fernandez, J. Arnold, D. Kinney, B. Laub, A. Makino, M. McGuire, K. Peterson, D. Prabhu, D. Empey, I. Dupzyk, L. Huynh, P. Hajela, P. Gage, A. Howard, and D. Andrews, “Adaptive Deployable Entry and Placement Technology (ADEPT): A Feasibility Study for Human Missions to Mars,” in *21st AIAA Aerodynamic Decelerator Systems Technology Conference and Seminar*. Dublin, Ireland: American Institute of Aeronautics and Astronautics, may 2011. [Online]. Available: <http://arc.aiaa.org/doi/10.2514/6.2011-2608>
- [4] R. R. Rohrschneider and R. D. Braun, “Survey of Ballute Technology for Aerocapture,” *Journal of Spacecraft and Rockets*, vol. 44, no. 1, pp. 10–23, 2007. [Online]. Available: <https://arc.aiaa.org/doi/pdfplus/10.2514/1.19288>
- [5] J. Slough, D. Kirtley, and A. Pancotti, “Plasma Magnetoshell for Aerobraking and Aerocapture,” in *32nd International Electric Propulsion Conference*, Wiesbaden, Germany, 2011. [Online]. Available: https://s3-us-west-2.amazonaws.com/pnwmsnw/MAC_IEPC-2011-304.pdf
- [6] D. Kirtley, “A Plasma Aerocapture and Entry System for Manned Missions and Planetary Deep Space Orbiters,” Tech. Rep., 2014.
- [7] B. G. Drake, S. J. Hoffman, and D. W. Beaty, “Human Exploration of Mars, Design Reference Architecture 5.0,” in *2010 IEEE Aerospace Conference*. IEEE, 2010. [Online]. Available: <http://ieeexplore.ieee.org/document/5446736/>
- [8] R. Bailey, J. Hall, T. Spilker, and N. O’Kongo, “Neptune Aerocapture Mission and Spacecraft Design Overview,” in *Joint Propulsion Conference and Exhibit*. Reston, Virginia: American Institute of Aeronautics and Astronautics, jul 2004. [Online]. Available: <http://arc.aiaa.org/doi/10.2514/6.2004-3842>
- [9] D. Kirtley, “ISS Launched CubeSat Demonstration of Variable-Drag Magnetoshell Aerocapture: Phase I Final Report,” Tech. Rep., 2014.
- [10] S. M. Hancock, R. W. Moses, and C. Goyne, “Magnetoshell Aerocapture Performance Opportunities at Mars,” in *2018 AIAA SPACE and Astronautics Forum and Exposition*, no. September, 2018, pp. 1–14. [Online]. Available: <https://arc.aiaa.org/doi/10.2514/6.2018-5313>
- [11] J. D. Jackson, *Classical Electrodynamics*. New York: John Wiley & Sons, Inc, 1962.
- [12] E. T. Meier and U. Shumlak, “A general nonlinear fluid model for reacting plasma-neutral mixtures,” *Physics of Plasmas*, vol. 19, no. 7, 2012.
- [13] M. A. Lieberman and A. J. Lichtenberg, *Principles of Plasma Discharges and Materials Processing*, 2nd ed., Hoboken, NJ, 2005.
- [14] R. J. Goldston and P. H. Rutherford, *Introduction To Plasma Physics*. Bristol and Philadelphia: Institute of Physics Publishing, 1995, vol. 01.
- [15] S. I. Braginskii, “Transport processes in a plasma,” 1965.
- [16] A. V. Phelps, “Cross Sections and Swarm Coefficients for Nitrogen Ions and Neutrals in N₂ and Argon Ions and Neutrals in Ar for Energies from 0.1 eV to 10 keV,” *Journal of Physical and Chemical Reference Data*, vol. 20, no. 3, pp. 557–573, 1991.

- [17] B. M. Smirnov, *Introduction to Plasma Physics*. Moscow: Mir, 1977.
- [18] Y. Itikawa, "Effective collision frequency of electrons in atmospheric gases," *The Physics of Fluids*, vol. 16, pp. 831–835, 1973.
- [19] K. G. Harstad, "Transport equations for gases and plasmas obtained by the 13-moment method - a summary," NASA Jet Propulsion Lab, Pasadena, CA, Tech. Rep., 1968.
- [20] J. D. Huba, *NRL Plasma Formulary*. Washington, DC: Naval Research Laboratory, 2011.

BIOGRAPHY



Charles L. Kelly is a NASA Space Technology Research Fellow and a PhD student in the department of Aeronautics & Astronautics at the University of Washington. He received his MS in Aeronautics & Astronautics from the University of Washington in 2018 and his BSE in Mechanical and Aerospace Engineering from Princeton University in 2014.



Justin M. Little is an Assistant Professor in the department of Aeronautics & Astronautics at the University of Washington and director of the SPACE Lab. He received his PhD in Mechanical and Aerospace Engineering from Princeton University in 2014 and his BS in Physics and Aerospace Engineering from the University of California Irvine in 2008.